JGR Atmospheres

RESEARCH ARTICLE
10.1029/2021JD036368

Terrestrial Gamma-Ray Flashes With Accompanying Elves Detected by ASIM

Ingrid Bjørge-Engeland[1], Nikolai Østgaard[1], Andrey Mezentsev[1], Chris Alexander Skeie[1], David Sarria[1], Jeff Lapierre[2], Anders Lindanger[1], Torsten Neubert[3], Martino Marisaldi[1,4], Nikolai Lehtinen[1], Olivier Chanrion[3], Kjetil Ullaland[1], Shiming Yang[1], Georgi Genov[1], Freddy Christiansen[3], and Victor Reglero[5]

[1]Department of Physics and Technology, Birkeland Centre for Space Science, University of Bergen, Bergen, Norway, [2]Earth Networks, Germantown, MD, USA, [3]National Space Institute, Technical University of Denmark (DTU Space), Kongens Lyngby, Denmark, [4]INAF-OAS Bologna, Bologna, Italy, [5]Image Processing Laboratory, University of Valencia, Valencia, Spain

Key Points:

- We present a sample of 17 Terrestrial Gamma-ray Flashes (TGFs) with accompanying Elves detected by Atmosphere-Space Interactions Monitor
- TGFs with Elves are short and associated with very high peak current lightning
- The peak currents for these events are higher than for both lightning and TGFs in general

Supporting Information:

Supporting Information may be found in the online version of this article.

Correspondence to:

I. Bjørge-Engeland,
ingrid.engeland@uib.no

Citation:

Bjørge-Engeland, I., Østgaard, N., Mezentsev, A., Skeie, C. A., Sarria, D., Lapierre, J., et al. (2022). Terrestrial Gamma-ray Flashes with accompanying Elves detected by ASIM. *Journal of Geophysical Research: Atmospheres*, *127*, e2021JD036368. https://doi.org/10.1029/2021JD036368

Received 16 DEC 2021
Accepted 23 MAY 2022

Abstract The Atmosphere-Space Interactions Monitor was designed to monitor Terrestrial Gamma-ray Flashes (TGFs) and Transient Luminous Events (TLEs) from space, enabling the study of how these phenomena are related. In this paper, we present observations of 17 TGFs with accompanying Elves. TGFs are short and highly energetic bursts of gamma photons associated with lightning discharges, whereas Elves are TLEs that are observed as concentric rings of ultraviolet (UV) and visible light at ionospheric altitudes, produced by the excitation of N_2 molecules when an electromagnetic pulse hits the base of the ionosphere. Elves were identified when optical detections in the UV band could be clearly distinguished from other optical signals from lightning strokes. The TGFs they accompanied had short durations and were associated with particularly high peak current lightning. Lightning sferics associated with these events were detected by the global lightning network GLD360 and the World Wide Lightning Location Network, and they were, with the exception of one event, observed over ocean or coastal regions. It is likely that these events were associated with Energetic In-cloud Pulses. We show that short duration TGFs tend to be associated with higher peak currents than long duration TGFs.

1. Introduction

Terrestrial Gamma-ray flashes (TGFs) are short and energetic (up to ~40 MeV) bursts of photons, produced by relativistic electrons in bremsstrahlung processes in the large electric fields in thunderclouds (Bethe & Heitler, 1934; Dwyer et al., 2012; Köhn & Ebert, 2014). The TGF photons experience Compton scattering and pair-production as they propagate through the atmosphere, before being detected by spacecraft in the inner parts of the magnetosphere (Dwyer et al., 2012). The first observations of TGFs from space were reported by Fishman et al. (1994), and since then they have been detected by several spacecraft. The properties of the Atmosphere-Space Interactions Monitor (ASIM), which is the first instrument specifically designed for observing TGFs, allow for studying the relationship between TGFs and other phenomena related to lightning discharges, namely Transient Luminous Events (TLEs). One of these phenomena is Elves (Emissions of light and Very Low Frequency (VLF) perturbations due to electromagnetic pulse (EMP) sources), which are observed as concentric rings of light, including ultraviolet (UV) and visible bands, at ionospheric altitudes that appear to be expanding laterally at speeds greater than the speed of light, due to the outer rings of the Elve being detected before the inner rings because of the viewing geometry. Elves are produced when EMPs from lightning encounter the lower ionospheric boundary and excite nitrogen (N_2) molecules in the ionosphere (Fukunishi et al., 1996; Inan et al., 1996, 1997).

TGFs observed from space are likely to be produced during positive intracloud (IC) lightning discharges, during the upward propagation of negative lightning leaders (Cummer et al., 2005; Heumesser et al., 2021; Lu et al., 2010; Pasko et al., 2012; Shao et al., 2010; Stanley et al., 2006; Østgaard et al., 2013). It has been suggested that the in-cloud discharge processes that produce TGFs can also produce Elves (Cummer et al., 2014; Liu et al., 2017). Elves are associated with high peak current events, and thresholds for Elve production have been suggested to be ~90 kA for cloud-to-ground (CG) lightning, through a combination of observations and simulations (Marshall et al., 2015). This is also described in a modeling study by Inan et al. (1996), where EMPs radiated by CG return strokes with peak currents >80 kA were found to be able to produce bright Elves. Chen et al. (2008) used data

from the Imager of Sprites and Upper Atmospheric Lightning experiment and observations of more than 5,400 Elves associated with CG flashes, and showed that ∼90% of Elves are associated with lightning discharges with peak currents >60 kA. Both Elves and high peak current (>80 kA) lightning have been reported to occur much more frequently over oceans and coastal regions than over land, but this has so far mainly been studied for negative CG strokes (Chen et al., 2008; Said et al., 2013). Although the strongest currents are found over ocean, lightning occurs much more frequently over land (C. Liu et al., 2010; Mach et al., 2010, 2011).

Recent research has suggested that when Energetic In-cloud Pulses (EIPs) are observed, it is very likely that a TGF is also produced. EIPs are typically produced during the upward propagation of negative lightning leaders, at altitudes of 10–13 km (Cummer et al., 2014; Lyu et al., 2015). The high currents associated with EIPs indicate that the EMPs they radiate can also produce Elves (Cummer et al., 2014; Lyu et al., 2015; Liu et al., 2017; Østgaard et al., 2021). For IC events, using data from the National Lightning Detection Network, Lyu et al. (2015) reported two types of discharges with observed peak currents >200 kA; Narrow Bipolar Events (NBEs) and EIPs. NBEs appear quite isolated, and are very short (∼10–20 μs) radio pulses from which a large range of peak current values can be derived. The most common are the -NBEs that occur close to cloud tops. EIPs have longer duration waveforms and are, as the name indicates, observed within the cloud and the derived peak currents are large (>60 kA). +NBEs are also observed within the cloud, but are shorter (∼10–20 μs) compared to EIPs (∼50–100 μs) (Lyu et al., 2015). Out of a total of 199 events with peak currents >200 kA, Lyu et al. (2015) identified 139 as IC events, where 67 were −NBEs, 69 +EIPs and 3 −EIPs. Combined with the timescales of EIPs, they suggest a connection between EIPs, TGFs and Elves. N. Liu et al. (2017) also suggest that Elves are more likely to accompany short duration TGFs, as a short TGF duration indicates a fast current change, which can produce an EMP. Short TGFs have a higher match rate with sferics (very low frequency radio atmospherics produced by lightning) detected by lightning detection networks as they emit more energy at the radio frequencies that are detected by the networks, around 10 kHz (Connaughton et al., 2013; Dwyer & Cummer, 2013; Lindanger et al., 2020).

The first observation of a TGF with an accompanying Elve was reported by Neubert et al. (2020), where the TGF and Elve were produced by the same IC lightning. Another TGF accompanied by an Elve was reported by Østgaard et al. (2021), where an EIP produced the optical lightning pulses associated with the TGF as well as the observed Elve. The small difference (10–20 μs) in onset times of the TGF and the UV signal is believed to be influenced by several different factors; instrumental sensitivity, signal noise and observational geometry, as well as the lifetime of the UV emission in the ionosphere and the steepness of the source current moment (Østgaard et al., 2021).

In this paper, we present observations of 17 TGFs by ASIM with accompanying Elves, detected between the launch of ASIM in 2018 and the end of 2020. Simultaneous observations of these events are possible because of ASIM's ability to monitor lightning, TGFs and TLEs, providing both gamma-ray detections and optical detections by photometers operating in three different wavelength bands. Using the detections from all three photometers, we were able to distinguish the optical signatures of Elves from the optical signatures from the lightning associated with the TGFs. Using data from Vaisala's global lightning database GLD360 we obtained information about the currents producing these unique events and determined the location of the associated lightning discharges. Data from the World Wide Lightning Location Network (WWLLN) allowed us to track the movement of the storm systems associated with these events over several hours. Using the observations from ASIM and associated sferic detections, both for the 17 events and for a large set of ASIM TGFs, we studied how these events are unique and how their properties compare to other TGFs.

2. Instruments and Data

2.1. ASIM

The ASIM payload is mounted on the Columbus module of the International Space Station (ISS), orbiting Earth at an altitude of ∼410 km and an orbital inclination of 51.6°. ASIM is mounted on the lower deck of the module, facing nadir (Neubert et al., 2019). The payload consists of the two instruments the Modular X- and Gamma-ray Sensor (MXGS) (Østgaard, Balling, et al., 2019) and the Modular Multi-spectral Imaging Array (MMIA) (Chanrion et al., 2019). MXGS is an imaging and spectral X- and gamma-ray instrument, with two detector layers; the

High Energy Detector (HED) and the Low Energy Detector (LED). MMIA is a suite of optical sensors, containing three photometers and two cameras, and is only operated during night-time (Chanrion et al., 2019).

LED consists of Cadmium-Zinc-Telluride (CZT) crystals, and a coded mask provides an 80° × 80° field of view (FOV). The CZTs are sensitive to photons with energies of 50–400 keV. LED has a temporal resolution of 1 μs (Østgaard, Balling, et al., 2019). HED consists of 12 Bismuth-Germanium-Oxide (BGO) detectors, each coupled to a photomultiplier tube, and it is mounted behind LED, shielding LED from radiation from the rear. HED is switched off during passage through the South Atlantic Anomaly to protect the PMTs against high particle fluxes. HED is sensitive to photon energies from 300 keV to >30 MeV. The temporal resolution of HED is 27.8 ns, and the deadtime of each BGO detector is 550 ns. MXGS is described in detail in Østgaard, Balling, et al. (2019).

The MMIA photometers operate in three wavelength bands; 337 nm (4 nm bandwidth), 180–230 nm (UV) and 777.4 nm (5 nm bandwidth), with a sampling rate of 100 kHz (Chanrion et al., 2019). The 337 and 777.4 nm photometers have a square 80°-diagonal FOV, while the UV photometer has a circular 80°-diameter FOV. Detections in 777.4 nm are dominated by the emissions from the lightning leader, whereas the other photometers can also detect signals from TLEs. Emissions in the 777.4 nm band originate from atomic oxygen, and emissions in 337 nm originate from a band in the second positive group of molecular nitrogen ($N_2 2P$). Emissions in UV are to a large extent absorbed by molecular oxygen in the air, and the signals can therefore be used to identify TLEs, which are produced at higher altitudes than lightning (Chanrion et al., 2019).

The MMIA cameras and photometers are co-aligned and mounted on an optical bench, with a tilt of 5° to avoid disturbances from another payload on the ISS (Chanrion et al., 2019). The UV photometer's circular FOV extends to ∼345 km from the nadir point on the Earth surface (the footpoint), and the other photometers are limited to ∼243 km at the sides of the square FOV (the 5° tilt, ∼35 km at surface, is not accounted for). The temporal resolution of the photometers is 10 μs. The optical designs of the 337 and 777.4 nm photometers are identical, and both contain an interference filter for limiting the wavelength shift of the photometers (Chanrion et al., 2019).

MXGS and MMIA have a cross-triggering system, but they can also trigger individually. MXGS captures 2 seconds of data when triggered, and sends a cross-trigger to MMIA (Østgaard, Neubert, et al., 2019). When MMIA detects signals above background variations, a cross-trigger is sent to MXGS, and 2 seconds of both MXGS and MMIA data are registered. The cross-triggering enables the capture of optical signals from lightning discharges associated with TGFs that occur within the MMIA FOV. The relative timing accuracy between MXGS and MMIA was ±80 μs between launch and 28 March 2019. After an onboard software update, the relative timing uncertainty between MXGS and MMIA was improved to ±5 μs. The absolute timing uncertainty of ASIM is [−10, 40] ms, due to the ISS clock.

2.2. Lightning Detection Networks

To determine the lightning source location and currents associated with coincident TGFs and Elves, we used data from the ground-based lightning detection networks GLD360 and WWLLN. To obtain information about the properties of the sferics associated with the TGFs and Elves, as well as with ASIM TGFs in general, we used data from GLD360. To study the evolution of specific storms we used data from WWLLN. Data from the Earth Networks Total Lightning Network (ENTLN) were used as a supplement to the GLD360 reports for some of the events.

For geo-locating lightning strokes, the ground-based networks use Time of Arrival (TOA) methods. GLD360 uses sensors in the 500 Hz − 50 kHz range and applies TOA methods in combination with a magnetic direction finding procedure (Said & Murphy, 2016). For the network to be able to geo-locate a lightning stroke, the event should be detected simultaneously by at least four different stations. Median location accuracy is ∼2.5 km for the United States (Rudlosky et al., 2017; Said et al., 2013). GLD360 does not distinguish between IC and CG discharges, but provides polarity values for the peak currents (Said et al., 2013). The network has a detection efficiency up of ∼60–80% for CG strokes over the United States (Said & Murphy, 2016; Said et al., 2010, 2013). WWLLN consists of sensors operating in the VLF range, and consists of >70 VLF-receiving stations globally. The detection efficiency of WWLLN varies, with the detection efficiency being lower over Africa and generally greater over oceanic regions, with an average global detection efficiency of 11% (Bürgesser, 2017; Hutchins et al., 2013; Rudlosky & Shea, 2013) and a location accuracy of 5 km (Hutchins et al., 2012). WWLLN is capable of detecting both CG and IC lightning strokes, and uses the time difference between the sferic detections at each

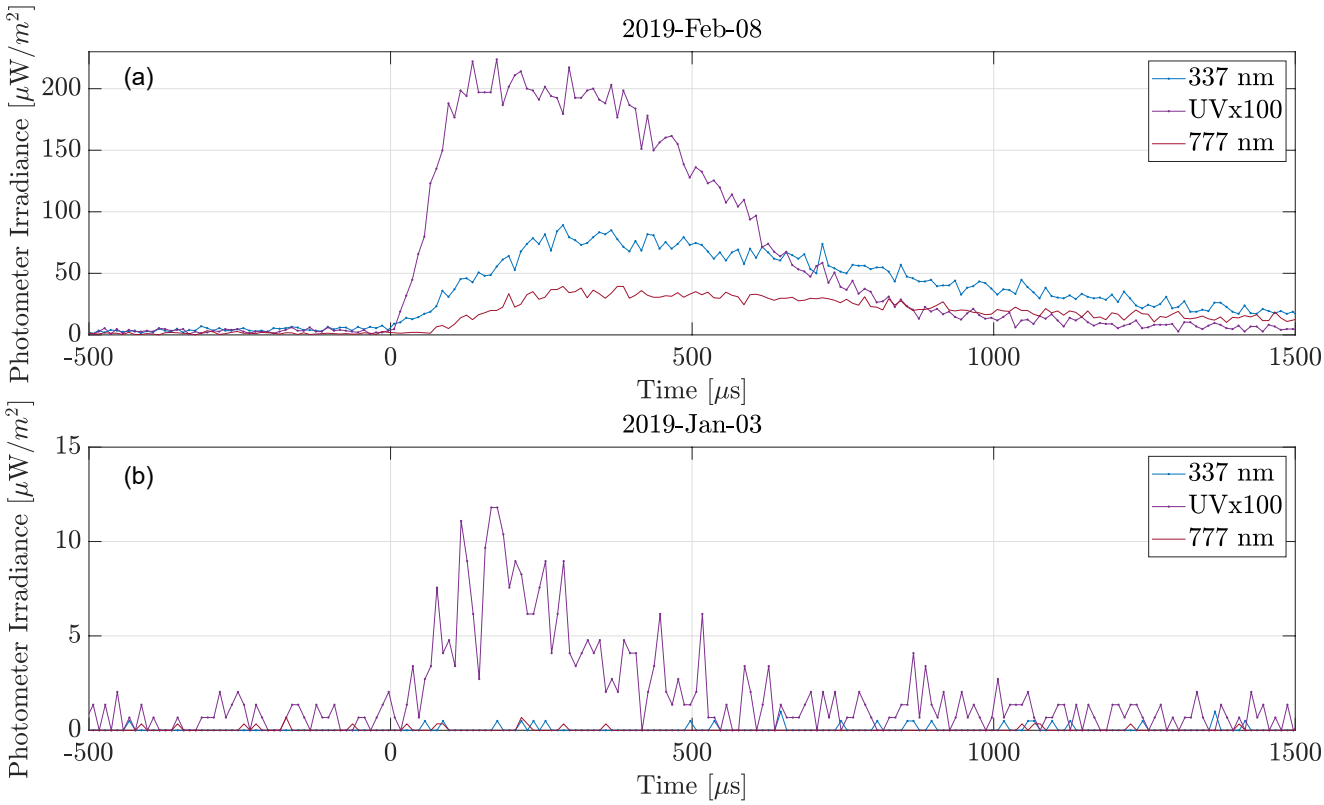

Figure 1. Photometer detections by MMIA for two ASIM TGFs with Elves. Time = 0 on the *x*-axis indicates the time of the first photon of the TGF detection by MXGS. The top panel shows photometer detections for Event 4 and the bottom panel for Event 3 in Table 2. The TGFs are plotted in the Supporting Information S1 (Figures S4 and S3).

receiving station to estimate the location of the lightning source. The ENTLN operates in wideband frequencies (1 Hz–12 MHz), and operates over 1,800 sensors globally, with the majority of the sensors being located in the United States. For locating the lightning discharges, ENTLN uses electric field waveforms, and TOA methods (Bui et al., 2015). ENTLN provides a classification of discharges in terms of CG and IC lightning and their polarities, by using wave shapes and electric field pulse polarities (Zhu et al., 2017).

For this study, we used a set of GLD360 sferic detections centered at ±1,000 s around ASIM TGF times restricted to a geographical area of 10° × 10° around the ISS footpoint. We obtained the timestamp of the GLD360 detection, provided down to nanosecond level, and the geographic location and peak current of the detection. WWLLN provides daily processed time-of-group-arrival data, and provides timestamps down to microsecond level of the lightning source time. From ENTLN we obtained information about peak current estimates for some of the TGFs with Elves, and the electric field waveforms obtained by the sensors.

3. Method

3.1. Identifying TGFs With Accompanying Elves

The initial search for TGFs with Elves consisted of finding all events with a pulse detection in the UV optical band. To identify whether the pulse originated from the lightning discharge itself or from an Elve, the pulse shapes detected by the three MMIA photometers were carefully inspected. The optical signals from lightning (in all three optical bands) are delayed and elongated by cloud scattering, while the signals from an Elve are unscattered when reaching the ASIM detectors. We therefore identified Elves when the UV signal reached its peak before the signals from lightning detected in the 337 and 777.4 nm bands (such as in Figure 1a). For the event in Figure 1a, the UV pulse has a very high intensity compared to UV signals associated with lightning discharges related to TGFs (such as in Figure 2). The associated sferic detection by GLD360 for the event in Figure 1a is

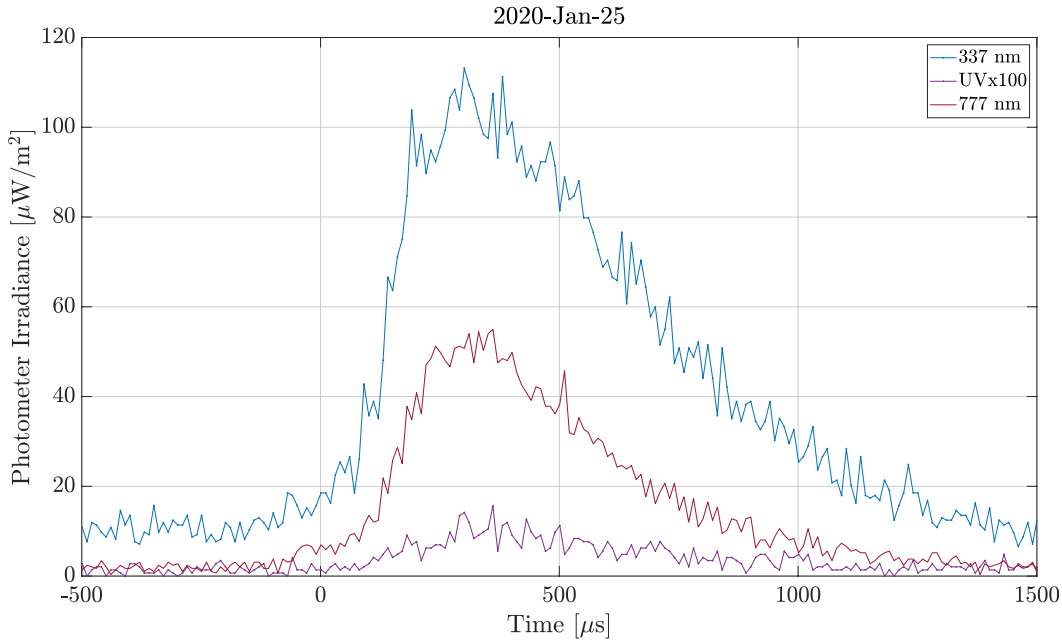

Figure 2. Photometer detections by MMIA accompanying an ASIM TGF, with signals from the lightning discharge detected by all three photometers (no Elve). Time = 0 corresponds to the time of the first photon of the TGF detection by MXGS.

located within the MMIA FOV, and a high peak current (257 kA) is associated with the event. For some events (such as Figure 1b), the UV pulse was the only optical pulse accompanying the TGF. These detections are inferred to originate from the expanding rings of an Elve centered outside the MMIA FOV, whose rings were able to expand into the FOV. A sferic with a high peak current was also found just outside the UV FOV within the time window [−10, 40] ms of the TGF detection, locating the parent lightning flash outside the UV FOV.

Figure 3 shows a more challenging case, where the three optical pulses had to be inspected more carefully to determine the origin of the UV detection. From the pulse shapes and the difference in onset times of the three optical pulses relative to the TGF onset time, the UV pulse could be seen to peak before the other pulses. All three pulses are weak, indicating a source close to the edge of the MMIA FOV. For this event and similar events, sferics

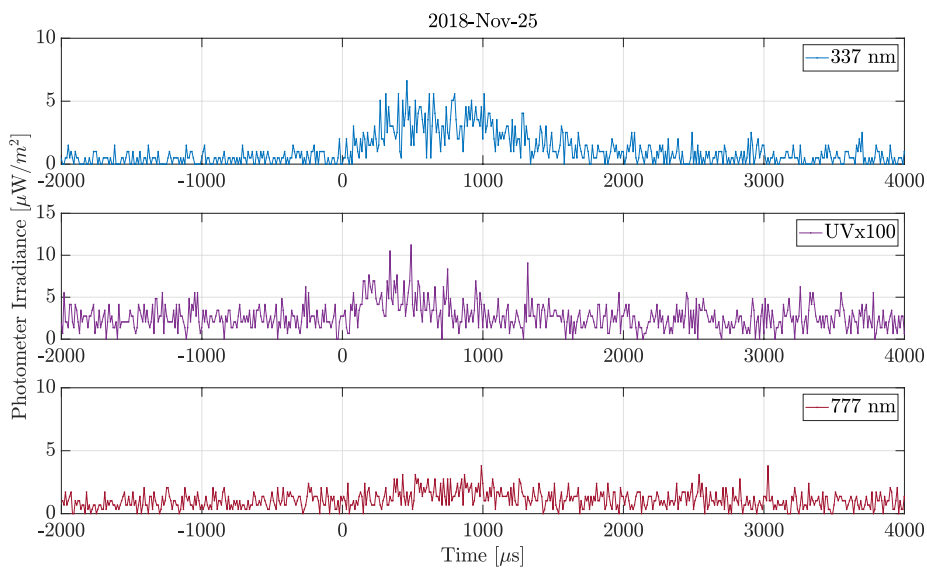

Figure 3. Photometer detections for an ASIM TGF with an accompanying Elve (Event 2 in Table 2). The panels show the detections in PHOTs 1–3, respectively. Time = 0 on the x-axis is the time of the first photon of the TGF detection by MXGS.

with strong peak currents were important for identifying the source location of the UV pulse, as strong EMPs are more likely to produce an Elve (Inan et al., 1991, 1996; Rowland et al., 1995).

To obtain information about the lightning discharges associated with the TGFs accompanied by Elves, we found the corresponding sferic detections by GLD360 (using the consistency check outlined in Section 3.2), that also provide peak current values for the events. Sferic locations were found using GLD360 for 15 of the 17 events, and WWLLN for the remaining two events. These locations were then checked against the TGF duration, number of counts and energies detected by HED, as part of a consistency check which will be explained in Section 3.2.

3.2. Geolocation of TGFs and Consistency Check

We compared the peak currents associated with the TGF-Elve pairs with the peak currents associated with other TGFs. Due to the timing uncertainty of ASIM, we searched for GLD360-detected sferics within $[-10, 40]$ ms (corrected for propagation time) of TGF detection times, and within 800 km from the ISS footpoint. We included 785 TGFs in this study, detected between launch and the end of 2020. We categorized the events into four different samples, with different levels of reliability of the TGF-sferic match:

Sample 1: Events where we could improve the timing accuracy down to ± 1.5 ms through time alignment of a sequence of GLD360 detections from within the MMIA FOV and within ± 2 s of the TGF detection, and several MMIA photometer pulses. Although the time alignment was performed for sferic detections inside the MMIA FOV, the time alignment of sequences also enabled us to find TGF/sferic matches within the MXGS FOV with an improved timing accuracy. The time alignment procedure is applied similarly as done by Maiorana et al. (2020) and Heumesser et al. (2021).

Sample 2: Events where only one GLD360 detection was found in the $[-10, 40]$ ms timewindow.

Sample 3: Events where there were several possible GLD360 detections that could be associated with the TGF.

Sample 4: Events where there were no possible sferic associations to the TGF.

We approximate the TGF duration by a core duration, using a sliding window to determine the shortest interval containing 90% of the HED counts associated with the TGF. This is what we will refer to as a "core duration." Before finding the core duration of the TGF, we identified the HED counts associated with the TGF and removed energetic particles. The associated counts were initially identified by requiring a <100 us separation between consecutive counts. This separation criterion could exclude some counts of long TGFs, and the events were therefore visually inspected to ensure all TGF HED counts were included before determining the core duration. Visual inspection led to small changes in duration for less than 10% of the TGFs.

For TGFs with possible sferic associations, we performed a consistency check between the TGF detection and the radial distance to the candidate sferics to get an indication of whether the TGF and a sferic were likely to be associated. We assume a TGF production half-cone of 30–40° (no tilt). As the consistency check, a combination of the following three properties of the TGF detection were considered:

1. *TGF duration*: Connaughton et al. (2013) and Lindanger et al. (2020) both showed that long duration TGFs are less likely to have associated sferic detections than short TGFs, and hence we expect it to be less likely that very long TGFs have associated sferic detections. This led to more caution when considering possible sferic matches for longer TGFs than for the shorter TGFs detected.
2. *TGF intensity*: Due to scattering processes in the atmosphere and the $1/r^2$-effect, we expect the number of counts detected by ASIM to be less for TGFs produced at large radial distances from the ISS footpoint (Gjesteland et al., 2011).
3. *TGF hardness*: If high energy counts (>10 MeV) are detected by HED, we expect the source location of the TGF to be at a short radial distance from the footpoint (Carlson et al., 2007; Hazelton et al., 2009; Østgaard et al., 2008). This is because only photons that have been Compton scattered and have reduced energies will be observed outside the initial angular distribution of photons, which was found to be 30–40° (Gjesteland et al., 2011). As shown in Figure 2 in Lindanger et al. (2021), the energy spectra of TGFs become softer when observed from a source location at a larger radial distance, and Gjesteland et al. (2011) showed that the softening of the TGF spectra is significant at observation angles >40°. Hence, we expect HED to detect photons with energies >10 MeV if the TGF is produced at a location within the MMIA FOV. As the initial angular distribution of high-energy gamma rays could be slightly tilted toward the ISS, detections of counts with energies >10 MeV were only used as an indicator for the TGF being produced inside the MMIA FOV.

Table 1
TGFs/GLD360 Sferics Samples

	Absolute timing	Sferic associations	Events after consistency check
Sample 1	±1.5 ms	Only one	78
Sample 2	[−10, 40] ms	Only one	349
Sample 3	[−10, 40] ms	More than one	109
Sample 4	[−10, 40] ms	None	249

If a TGF had a possible sferic association at a location from the footpoint that failed the consistency checks, the sferic was discarded. The TGF presented in Figure 4 is an example where the possible sferic associations failed the consistency check. The HED detected nine counts with energies >10 MeV, suggesting that the TGF was produced inside the MMIA FOV, and the 337 and 777.4 nm pulses detected by MMIA support this. However, the only possible sferic associations for this event (within the [−10,40] ms time window) were located at 500–600 km from the ISS footpoint, and hence the possible sferic associations were discarded for this event, and the TGF was sorted into Sample 4.

By applying the consistency check for each event in Samples 1, 2, and 3, we found likely sferic associations for 536 TGFs. The events that failed the consistency check were added to Sample 4. The resulting number of events in the samples are presented in Table 1. Sample 4 contains TGFs with no detected sferics or TGF-sferic matches that did not pass the consistency check. In addition, it contains 34 TGFs where time alignment of sferics and MMIA data resulted in no sferic matches for the TGF time (±1.5 ms). Time alignment of sferics and MMIA data greatly improved the absolute timing and Sample 1 is therefore the most reliable sample.

3.3. Analysis and Comparison of Peak Currents

To determine how the peak current values for the sferics associated with the TGFs and Elves compare to other peak current values detected by GLD360, we used a large sample of sferic detections. The sferic detections were sampled at ±1,000 s around ASIM TGF times and restricted to a geographical area approximately ±10° around the ISS footpoint at the time of TGF detection. To study if there were any differences in the peak currents over coastal, ocean and land regions, the detections were separated on their distances to the shoreline. This was done using the Global Self-consistent, Hierarchical, High-resolution Geography Database, providing a pre-calculated grid of distances to shorelines (https://www.soest.hawaii.edu/wessel/gshhg/). Coastal detections were defined to be within ±150 km of the shoreline, to be consistent with Albrechtsen et al. (2019) and Lindanger et al. (2020).

4. Results

4.1. TGF-Elve Properties

Following the criteria outlined in Section 3, we identified 17 TGFs with Elves between the launch of ASIM in April 2018 and the end of 2020. Table 2 shows the TGF core duration, the location of the associated sferic detection (which was found using GLD360 for 15 events and WWLLN for two events), the distance from the sferic location to the ISS footpoint at the time of the TGF detection, and the peak current recorded by GLD360. The geographical distribution of the events is shown in Figure 5. MXGS and MMIA observations of all the events are shown in Supporting Information S1. Eleven events occurred over ocean, five over coastal regions, and one over land (~330 km from the shoreline). The event located over land occurred in a lightning-intense region in Colombia, close to tall mountain regions, in a thundercloud cell with little movement away from its origin.

Some properties of the 17 TGF-Elve pairs are presented in Figure 6. The TGFs all had short core durations of less than 75 μs (Figure 6a), and were associated with high peak currents of typically several hundred kA (Figure 6b). Figure 6b shows the span in peak current values, with the highest values being close to 500 kA and a median peak current value (red line) of 270 kA. Figure 6c shows the relative intensities of the UV pulses produced by the Elves versus distance from the ISS footpoint to the sferic location. The blue line indicates the edge of the FOV of the UV photometer. The events with strong UV pulse detections by MMIA were associated with sferic locations close to the ISS footpoint, with the weakest pulse detections originating from Elves produced either toward the edge or outside the MMIA FOV.

As shown in Figure 6c, two of the events (event 3 and 5) occurred far outside the MMIA FOV, also when taking the 5° tilt into account (at ~460 and 440 km from the ISS footpoint). These events were associated with the highest peak current values among the 17 TGFs. The UV photometer detected signals from rings of the Elve expanding into the MMIA FOV. The photometer detections for these two events are shown in Figure 1b and in

Table 2
TGFs With Accompanying Elves

Event	TGF time	T_{core90} [μs]	Sferic location (lat, lon)	Sferic radial distance [km]	GLD360 Peakcurrent [kA]
1	2018-Oct-10-13:01:33	48	(1.08, 126.50)	250	-
2	2018-Nov-25-07:57:03	49	(5.88, −74.28)	299	195
3	2019-Jan-03-01:53:28	34	(3.99, −23.77)	462	466
4	2019-Feb-08-00:01:37	24	(25.78, −57.66)	84	257
5	2019-Jul-02-19:46:14	35	(−2.30, 63.98)	437	486
6	2019-Nov-01-04:34:37	39	(22.38, −49.34)	283	393
7	2019-Nov-19-17:13:24	57	(13.89, 158.48)	311	-
8	2020-Mar-27-04:28:27	43	(28.12, −61.05)	252	274
9	2020-Apr-28-10:08:15	37	(7.33, −126.53)	185	221
10	2020-May-27-14:38:02	41	(−15.50, 178.33)	289	76
11	2020-Jul-01-15:54:16	73	(9.34, 124.67)	90	348
12	2020-Jul-19-10:15:23	60	(15.01, −94.59)	170	285
13	2020-Aug-03-12:27:40	59	(19.49, 139.39)	207	398
14	2020-Aug-05-03:11:00	61	(12.00, −87.82)	304	392
15	2020-Sep-02-05:37:11	55	(20.63, −82.22)	105	155
16	2020-Sep-20-04:32:21	26	(28.48, −34.23)	61	269
17	2020-Nov-10-09:16:42	56	(13.37, 168.35)	177	249

Figure 7. For the event presented in Figure 7 (event 5), GLD360 reported a sferic located ∼440 km from the ISS footpoint, with a peak current of 486 kA. The onset of the UV pulse (where there was a sharp increase above the background signal) occurred ∼90 μs after the TGF onset. The TGF had a short core duration of 35 μs, consistent with the high peak current (Dwyer & Cummer, 2013; N. Liu et al., 2017). One event with a very intense UV pulse, from a source inside the MMIA FOV, is shown in Figure 8. For this event, the associated sferic was located by GLD360 ∼170 km from the ISS footpoint, with a peak current of 285 kA. The core duration of the TGF was 60 μs, and HED detected counts with energies >10 MeV, consistent with a source within the MMIA FOV. In comparison, for the event in Figure 7, which originated from outside the MMIA FOV, HED detected no counts with energies >10 MeV. The highest detected photon energy was ∼8 MeV, consistent with observing a TGF from outside the beaming angle of the TGF. As seen in Figure 8, the UV pulse has an onset before the 777 nm pulse, which is delayed due to scattering in the cloud.

As shown in Figure 6, the TGF-Elve pairs were associated with very high peak current values. This was also confirmed by peak current values obtained from ENTLN. Energy estimates by WWLLN associated with the TGFs accompanied by Elves further supported that these events are associated with sferics with higher energies than the general stroke detections by the networks. Peak current values for a large sample of sferic detections ($\sim 4 \times 10^6$) by GLD360 within ±1000 s of TGF detection times are presented in Figure 9, and the 15 TGF-Elve pairs with associated GLD360 sferics all fall into the highest end of the distribution with positive polarity. To investigate this further, we separate the sferics into ocean, land and coastal events (Figure 10). Compared to a large set of GLD360 sferic recordings from the three different regions, the sferics associated with the TGF-Elve pairs are all in the high end of the main distributions. This is especially evident for sferic detections over ocean.

4.2. Storm Evolution

Using sferic detections by WWLLN, we can track the evolution of the storms where the TGFs and Elves were produced. Figure 11 shows the evolution of three of the storm systems. For the events in Figure 11a (event 12) and Figure 11b (event 8), the storms developed in the hours leading up to the TGF and Elve production. For the event in Figure 11a, the storm initially started by the shore, and gradually moved outwards over the ocean. One of the other TGFs with an Elve (event 14) was also produced on the west-side of Central-America, and there was

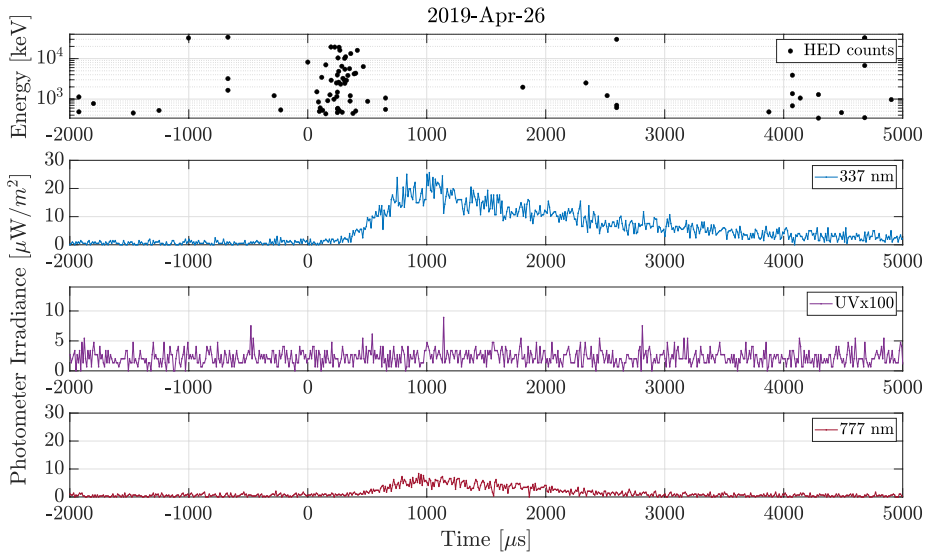

Figure 4. An example of a TGF likely to have been produced inside the MMIA FOV, with a significant number of counts with energies >10 MeV, where no matching sferic was found. The top panel shows the detections by HED for the event, and the three lower panels show the MMIA photometer detections following the TGF. Time = 0 on the *x*-axis marks the time of the first photon of the TGF detection.

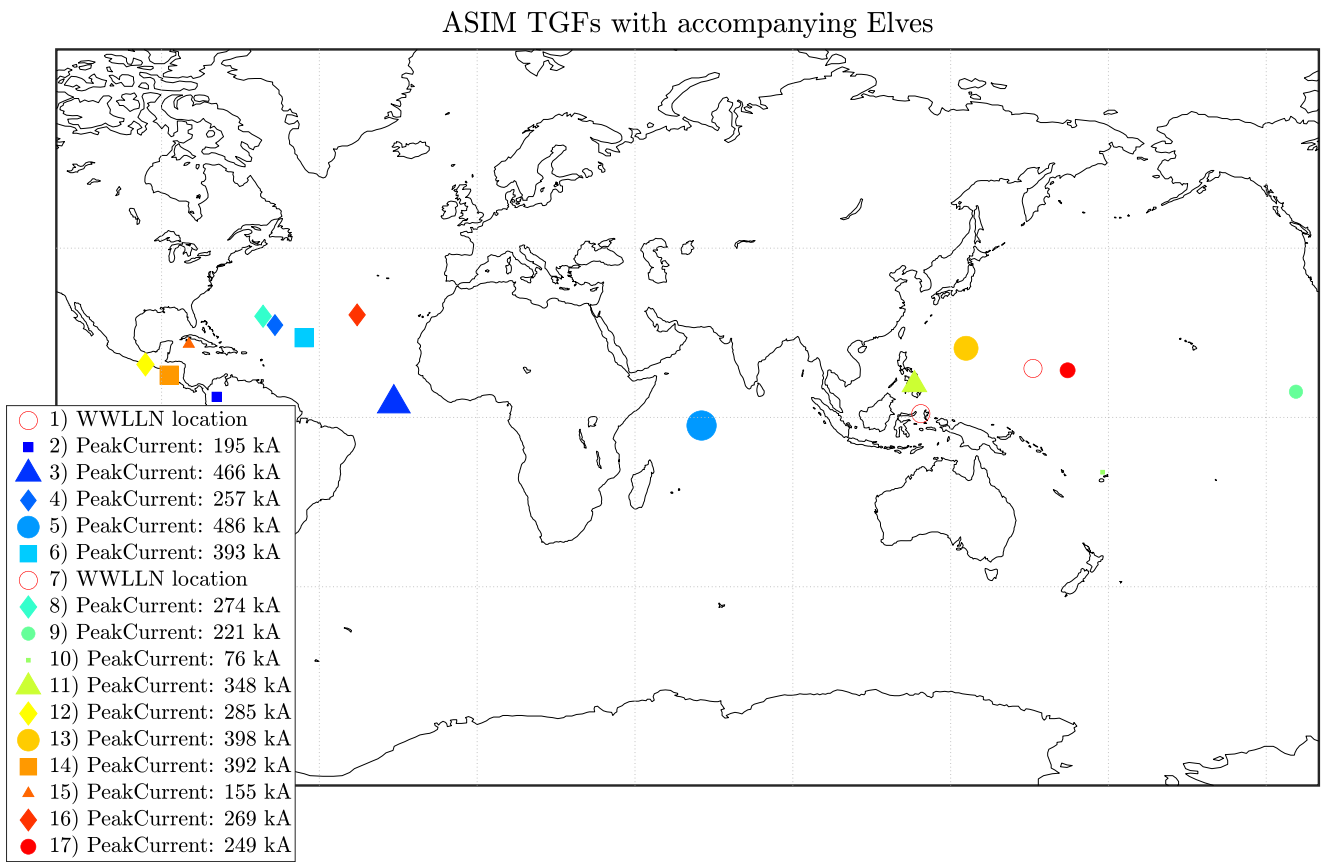

Figure 5. The locations of the Atmosphere-Space Interactions Monitor (ASIM) Terrestrial Gamma-ray Flashes (TGFs) with accompanying Elves, detected between launch and the end of 2020. The locations are given by the coordinates of the GLD360 associations for each event, with the exception of two events with no associated GLD360 detection, for which the location of the likely sferic association is provided by World Wide Lightning Location Network (WWLLN).

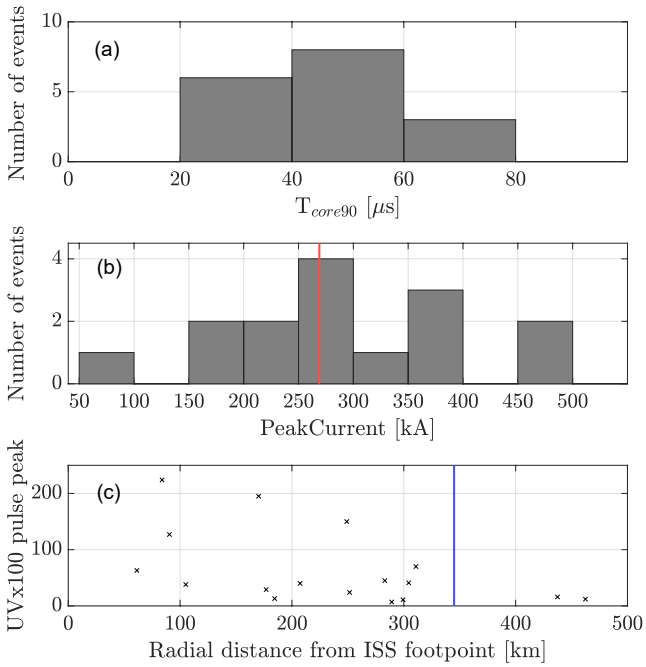

Figure 6. Properties of the ASIM TGFs with Elves. (a) Distribution of TGF core duration. (b) Distribution of GLD360 peak current values associated with the events. The red line indicates the median value. (c) Ultraviolet (UV) pulse peak intensity versus radial distance from the International Space Station (ISS) footpoint to the sferic source location. The blue line shows the edge of the FOV of the UV photometer (no tilt included).

a similar storm movement outwards from the coast. The event in Figure 11b (event 8) is categorized as an ocean event, and the storm moved gradually eastward. For both these events, the storms continued their movement after the production of the TGF and Elve. The storm system in Figure 11c, in which event 2 was produced, appears more isolated than the other storm systems. Further south (~100 km) of this storm cell, a different storm developed gradually over several hours. There was also another storm cell close to where the TGF was produced that faded a few hours before the TGF occurred. A storm cell at the TGF location started developing approximately 15 min before the TGF detection, and the cell continued to be active in the hours after the TGF occurred. However, it does not show any significant movement, in contrast to the events in Figures 11a and 11b. For the majority of the TGFs with Elves, the storm systems where they were produced developed before and after the event occurred. For some of the TGF-Elve pairs, the events were detected early in the storm cell development, and some events were detected over remote regions where the storm cells appeared quite isolated.

4.3. TGF Duration and Peak Current

In Figure 12, we present the distribution of the core durations of TGFs with associated GLD360 sferics (in red) compared to a distribution of core durations of the full set of 785 TGFs (in blue). In Figure 12a we present only the most reliable TGF-sferic matches (Sample 1 and 2, as outlined in Section 3.2), whereas we in Figure 12b use all three samples of TGF-sferic matches. The asterisks indicate the fraction of events within each duration bin with associated sferics. When using all three samples of sferic associations, there is a matchrate of >80% for the shortest TGFs, with the matchrate dropping to <30% for the longest TGFs.

Figure 13 shows the distribution of the core durations for the ASIM TGFs, and how the TGFs with Elves (in red) fall into the shortest duration end of this distribution. The median core duration for the set of 785 ASIM TGFs was found to be ~94 µs. All the core durations of the TGFs with Elves are below this value, with the longest duration for these events being ~73 µs, and a median core duration of 48 µs.

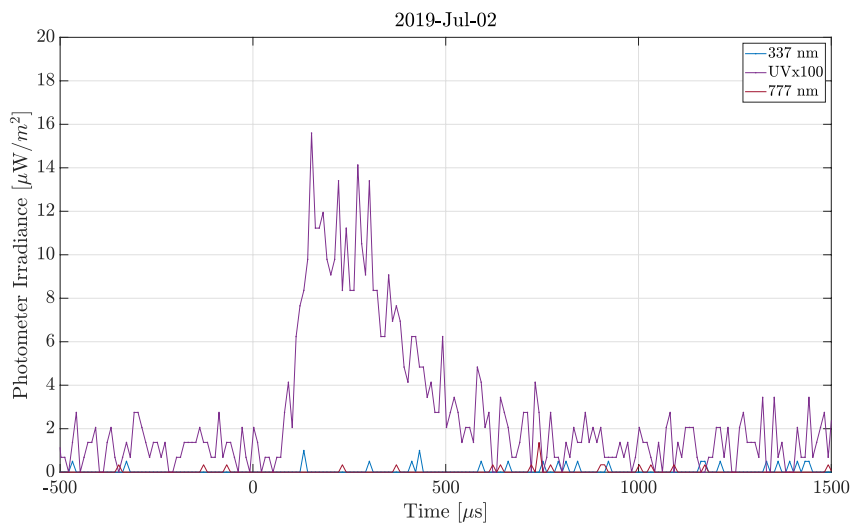

Figure 7. Photometer detections in 337 (blue), ultraviolet (UV) (purple) and 777.4 (red) nm for Event 5, produced outside the MMIA FOV. The HED detection of the TGF is shown in Figure S5.

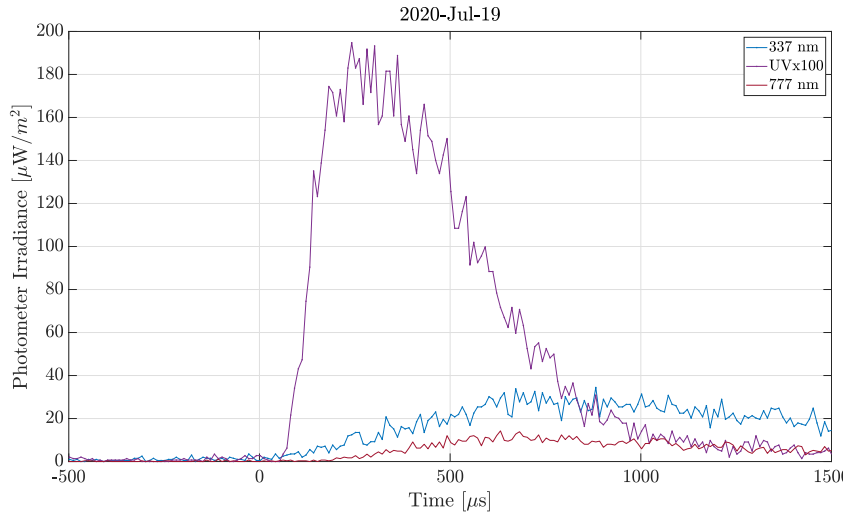

Figure 8. Photometer detections in 337 (blue), ultraviolet (UV) (purple) and 777.4 (red) nm for Event 12, with a strong UV pulse. The HED counts are shown in Figure S12.

The absolute value of the peak currents associated with the 536 ASIM TGFs (Samples 1, 2, and 3 in Table 1) are in Figure 14 compared to the large set of GLD360 peak currents presented in Figure 9. We used absolute values because the negative polarities could be due to a misreported polarity by the network, or because the network in some cases report only the ionospheric reflection instead of the ground wave (Cummins et al., 2008; Said et al., 2013). Each bin gives the (normalized) fraction of events in the set (blue or red) with a designated peak current. Both distributions show more events with lower peak current values, and a decrease in events toward higher peak current values. However, a larger fraction of events in the large set of GLD360 sferics have lower peak current values than those associated with the ASIM TGFs. The median peak current for the large set of GLD360 sferics was 10 kA (using absolute values), while for the sferics associated with the ASIM TGFs the median peak current was 39 kA (using absolute values). The corresponding mean values (also using absolute values) of the peak currents was 16 kA for the large set of GLD360 sferics and 74 kA for the sferics associated with the TGFs.

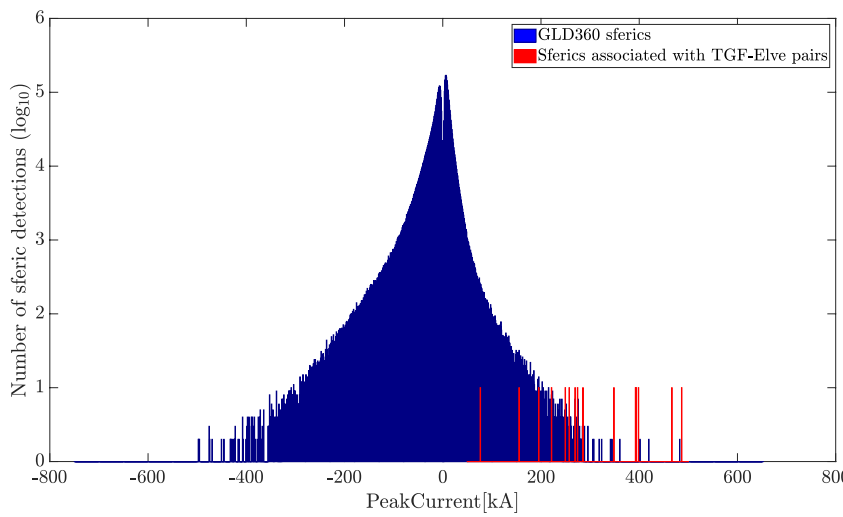

Figure 9. Log distribution of GLD360 peak current values from a sample of GLD360 sferics from 2020, centered at ±1,000 s around ASIM Terrestrial Gamma-ray Flash (TGF) times and ±10° around TGF location. The red bars indicate the peak currents associated with the TGFs accompanied by Elves.

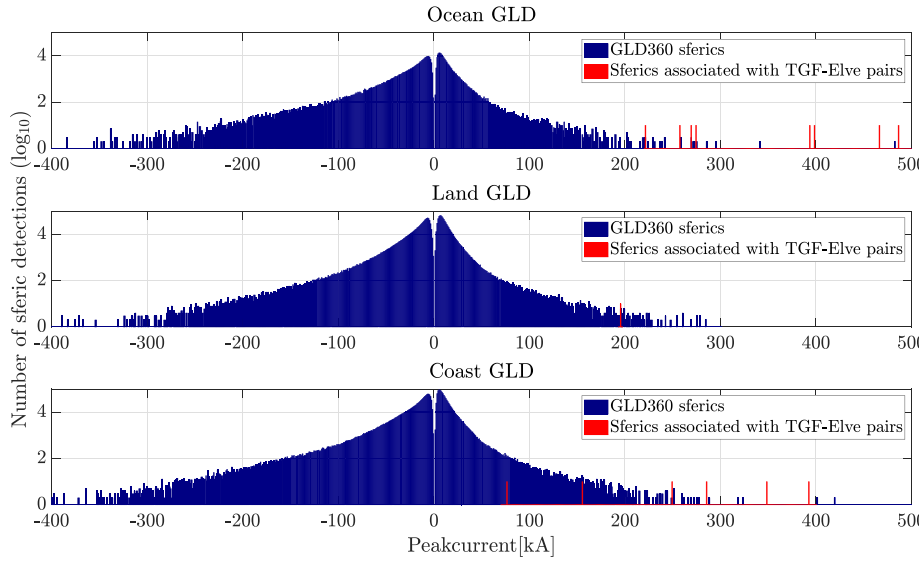

Figure 10. Log distribution of GLD360 peak current values from a sample of 2020 GLD360 detections, centered at ±1,000 s around ASIM Terrestrial Gamma-ray Flash (TGF) times and ±10° longitude and latitude around TGF locations, separated into ocean, land and coast events. The red bars indicate the peak current values associated with the TGFs accompanied by Elves.

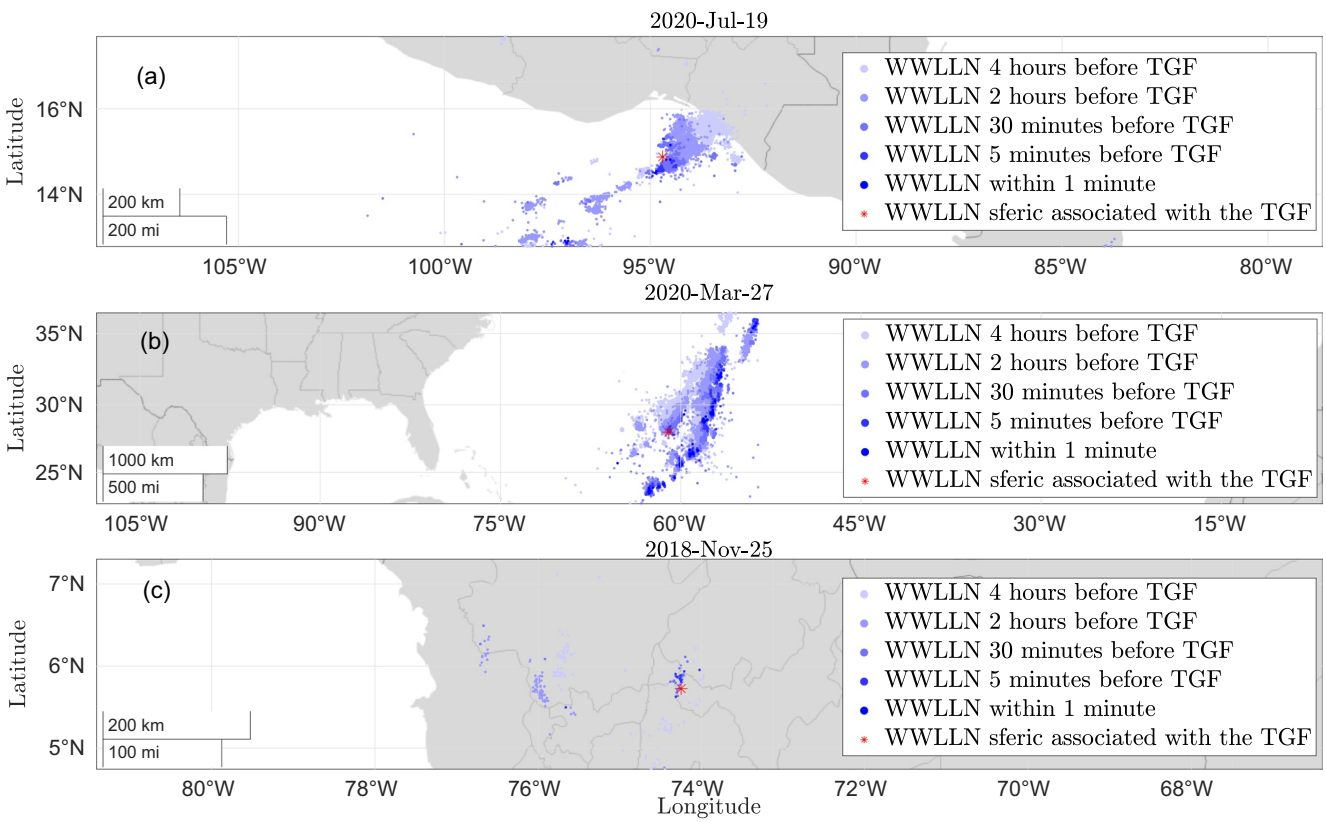

Figure 11. Evolution of three storms where a Terrestrial Gamma-ray Flash (TGF) and an Elve were produced, using sferics detected by World Wide Lightning Location Network (WWLLN). Increasing blue color indicates closeness to the time of the TGF detection. (a) A coastal event (event 12), with the WWLLN sferic associated with the TGF located at (14.87,−94.70). (b) An event (event 10) over ocean, with the WWLLN sferic associated to the TGF located at (28.01,−60.98). (c) The one event (event 2) detected over land, with a WWLLN sferic from (5.73,−74.25).

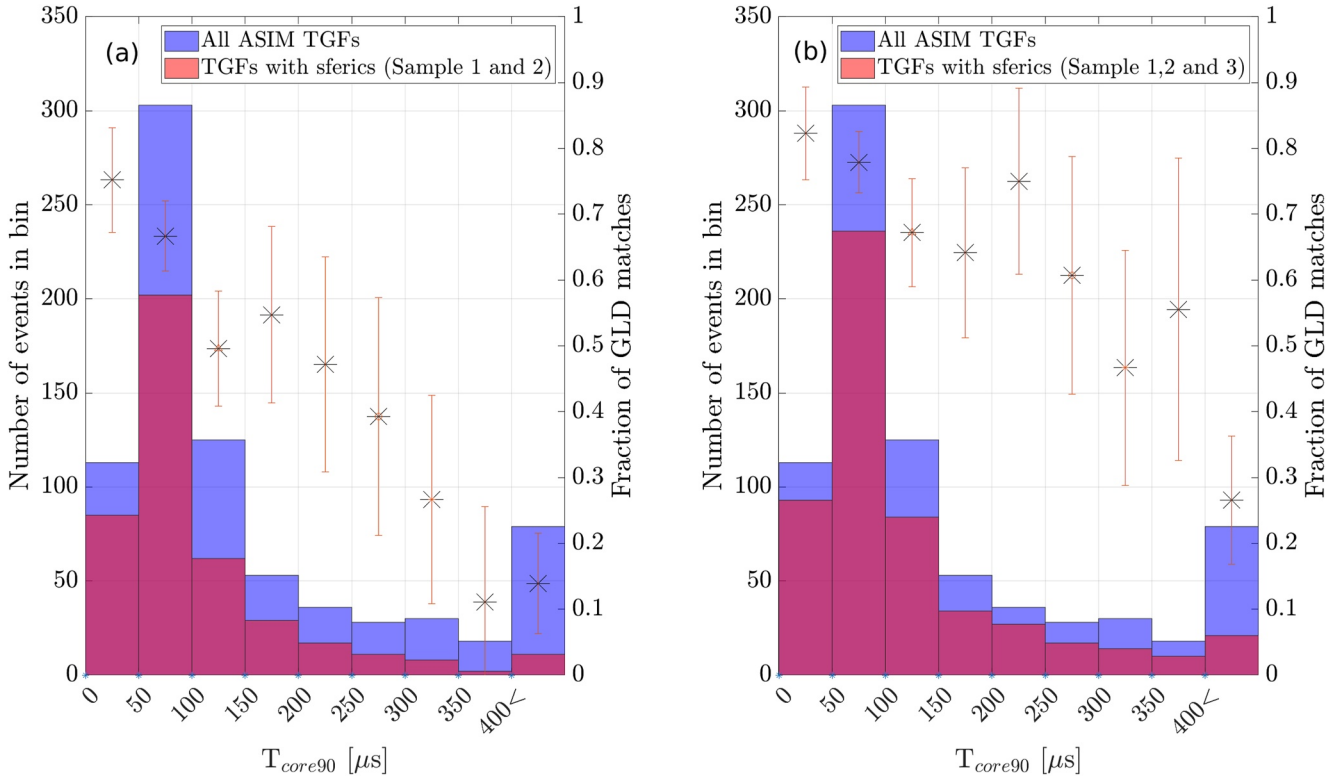

Figure 12. Distribution of Terrestrial Gamma-ray Flash (TGF) core durations for the full sample of Atmosphere-Space Interactions Monitor (ASIM) TGFs (785), with the TGFs with associated sferics highlighted by red bars. The asterisks are the fraction of events within each duration bin having an associated GLD360 sferic. The errorbars represent the 95% confidence interval. (a) The red bars include Samples 1 and 2 only. (b) The red bars include all TGFs in Samples 1, 2, and 3.

Figure 15a shows how the peak currents associated with ASIM TGFs (536 TGFs, Samples 1, 2, and 3) vary with distance from the shoreline. The TGFs associated with the highest peak currents were detected over ocean. The TGFs with sferics are separated into two sets; events with peak currents above and below the median (absolute value) peak current (39 kA). The distributions of events with distance to the shoreline for both sets are presented

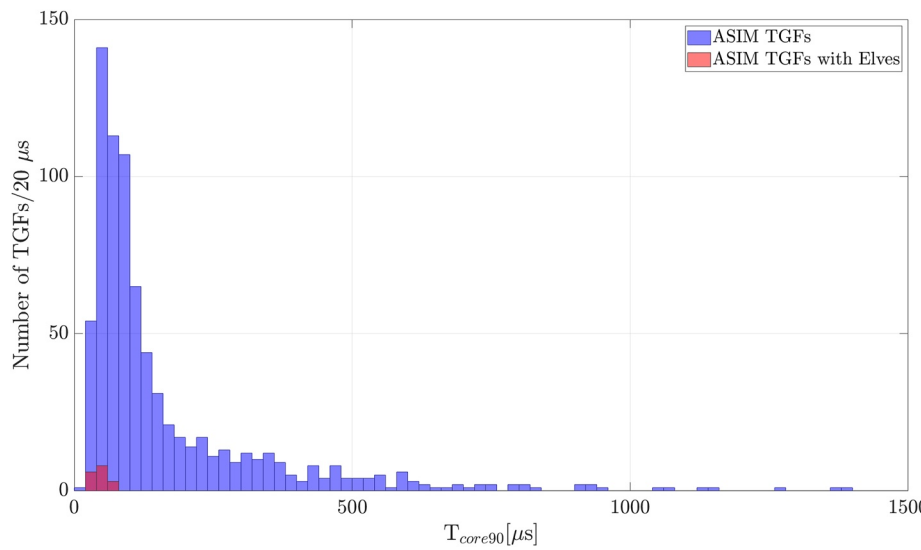

Figure 13. Distribution of Terrestrial Gamma-ray Flash (TGF) core duration for a set of (785) TGFs detected by Atmosphere-Space Interactions Monitor (ASIM) before the end of 2020 (blue), and the core duration for the 17 events with Elves (red). One event has a core duration of ~3,000 μs, not displayed in this figure.

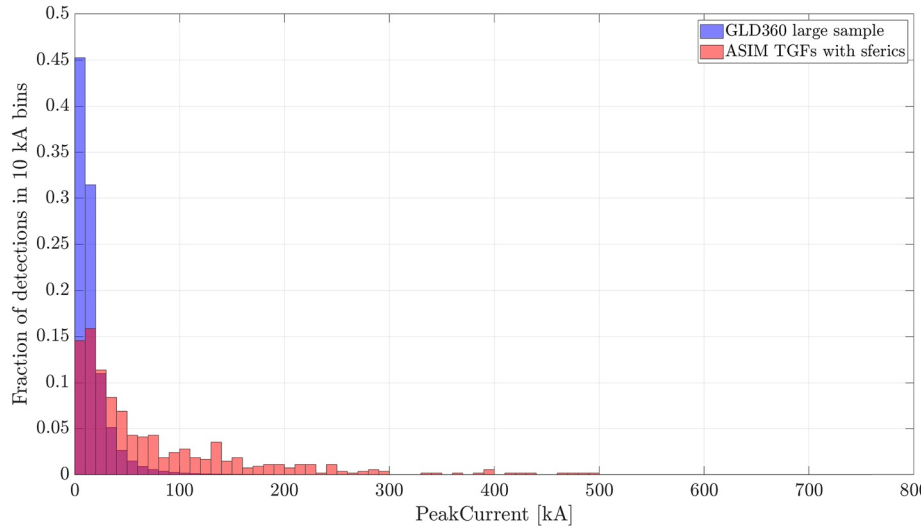

Figure 14. Distribution of GLD360 peak current detections (using absolute values), sorted in 10 kA bins. The blue bars are the peak currents from the large sample of GLD360 detections, where the amounts were normalized such that each bar gives the fraction of events relative to the full sample. The red bars are the peak currents associated with the Atmosphere-Space Interactions Monitor (ASIM) Terrestrial Gamma-ray Flashes (TGFs) (Samples 1, 2, and 3). These bars have also been normalized in the same manner, with the sum of the red histogram count values being equal to 1.

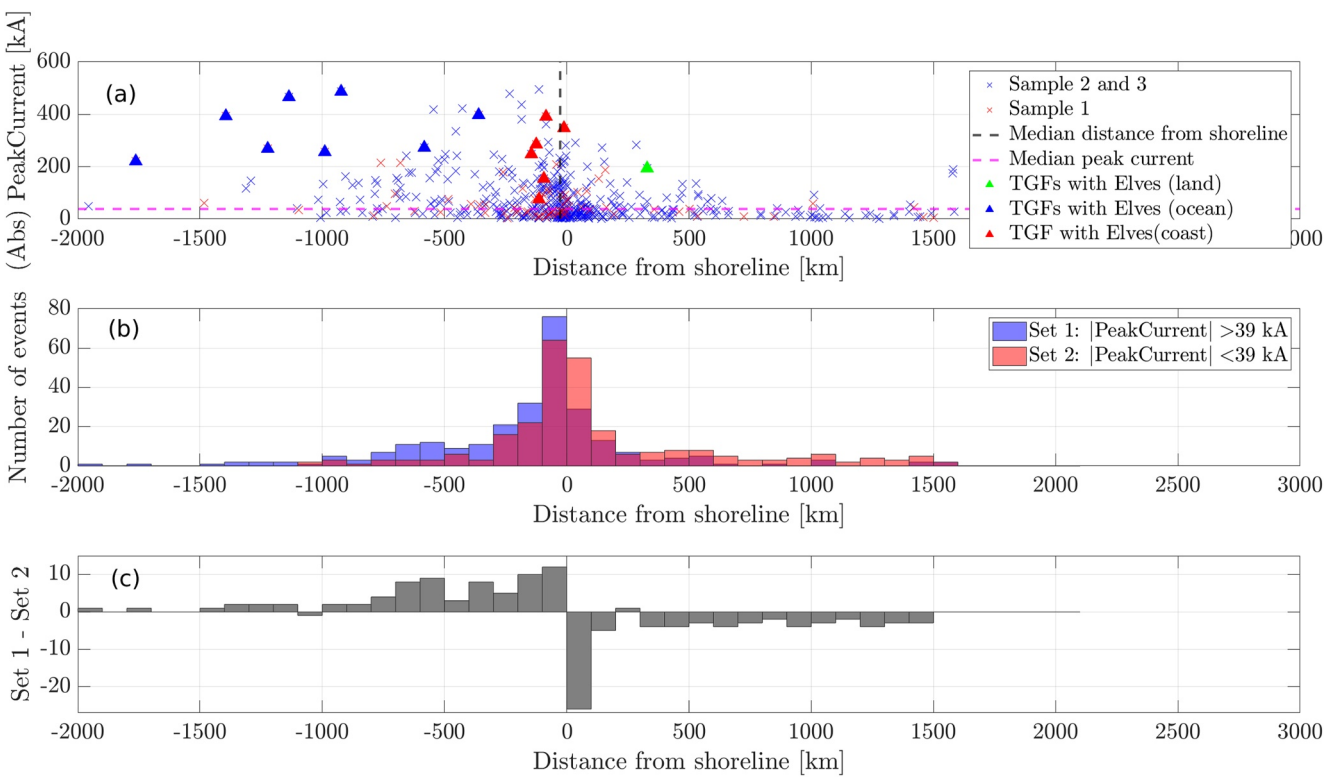

Figure 15. (a) Peak current (absolute values) versus the distance from the shoreline to the sferic location associated with the ASIM Terrestrial Gamma-ray Flashes (TGFs) (Samples 1, 2, and 3). Negative distances are over oceans. Green, blue, and red triangles are TGFs/Elves over land, ocean and coast, respectively. The magenta line represents the median peak current, and the vertical gray line represents the median distance from the shoreline. (b) Distributions of the distance to the shoreline (binwidth 50 km) for two intervals of peak current. Set 1 includes events with peak currents above the median value for the TGFs with sferics (Samples 1, 2, and 3), and Set 2 includes events with peak currents below the median. (c) The difference between Set 1 and 2 with distance from the shoreline.

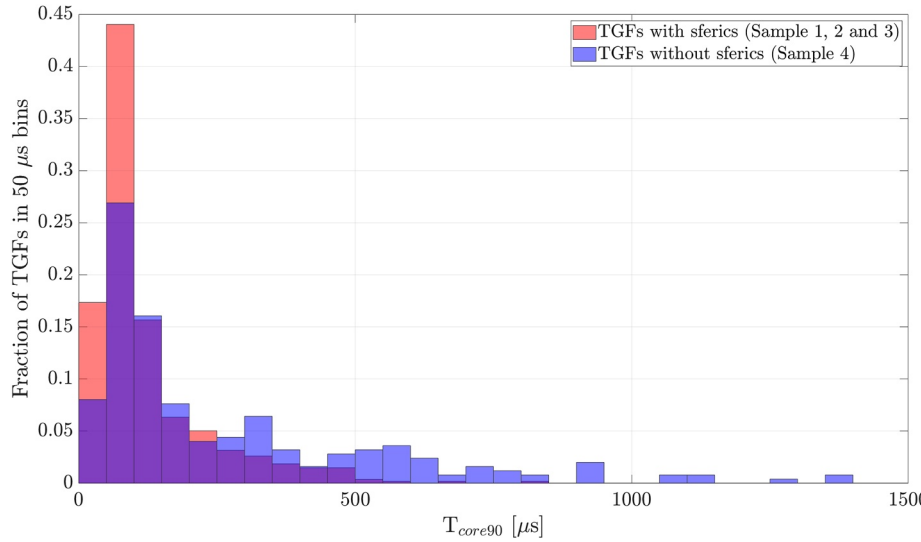

Figure 16. Distribution of core durations for the Terrestrial Gamma-ray Flashes (TGFs) without sferics (Sample 4) is presented in blue, and the distribution for the TGFs with sferics (Samples 1, 2, and 3) is presented in red. An outlier at ∼3,000 μs is not displayed in this figure.

in Figure 15b. The difference between the two sets (Set 1–Set 2) in each distance bin is presented in Figure 15c. This indicates that the high peak current sferics associated with TGFs tend to be detected over coastal regions and over ocean, which is where the sferics associated with the TGF-Elve pairs are also located.

To explore whether the TGFs without sferic matches (Sample 4) have a different core duration distribution than those with sferic matches (Samples 1, 2, and 3), the two distributions of core durations are presented in Figure 16. The distributions are similar to the full distribution of TGF durations for all the ASIM TGFs, in that the bins with shortest core durations contain far more events than the longer durations bins. However, a larger fraction of the TGFs in Sample 4 are shifted toward longer durations. The median core duration of the events in Sample 4 is ∼147 μs, whereas it was ∼94 μs for the full sample of ASIM TGFs (785 events). In comparison, for the TGFs with associated sferics (Samples 1, 2, and 3), the median core duration was ∼84 μs.

In Figure 17, we present a log-log scale scatter plot of (absolute value) GLD360 peak currents versus TGF core duration for TGFs with sferics (Samples 1, 2, and 3, see legend for color coding), as well as the events with Elves (red triangles). A linear regression line was fitted to the points in Samples 1, 2, and 3. For all three samples, there is a clear trend that the peak currents associated with the shorter TGFs are higher than those associated with the longer TGFs. The subset of events with Elves remains in one area of Figure 17d, with short core durations and particularly high peak current values.

The median peak currents for different TGF core duration-intervals, corresponding to the 25th and 75th percentiles of the durations of the TGFs with sferics (Samples 1, 2, and 3), are presented in Table 3 (using absolute values). The correlation coefficients between the logarithmic values of TGF core duration and peak current values for the three samples (Table 4), demonstrate only minor differences between the samples. Sample 2 is the largest sample and has the shortest confidence interval. The trend observed indicates a power law relationship between the TGF core duration and peak current.

5. Discussion

Using ASIM's ability to monitor both TGFs and TLEs, we studied in detail a group of 17 TGFs accompanied by Elves. We found sferic detections by GLD360 for 15 of these events, providing information about the lightning source location, as well as the peak current of the lightning discharge. For the remaining two events, the associated lightning location was found using sferic detections by WWLLN. The peak current values associated with the TGF-Elve pairs were compared to a large set of peak current values from lightning strokes as well as with a large sample of other ASIM TGFs.

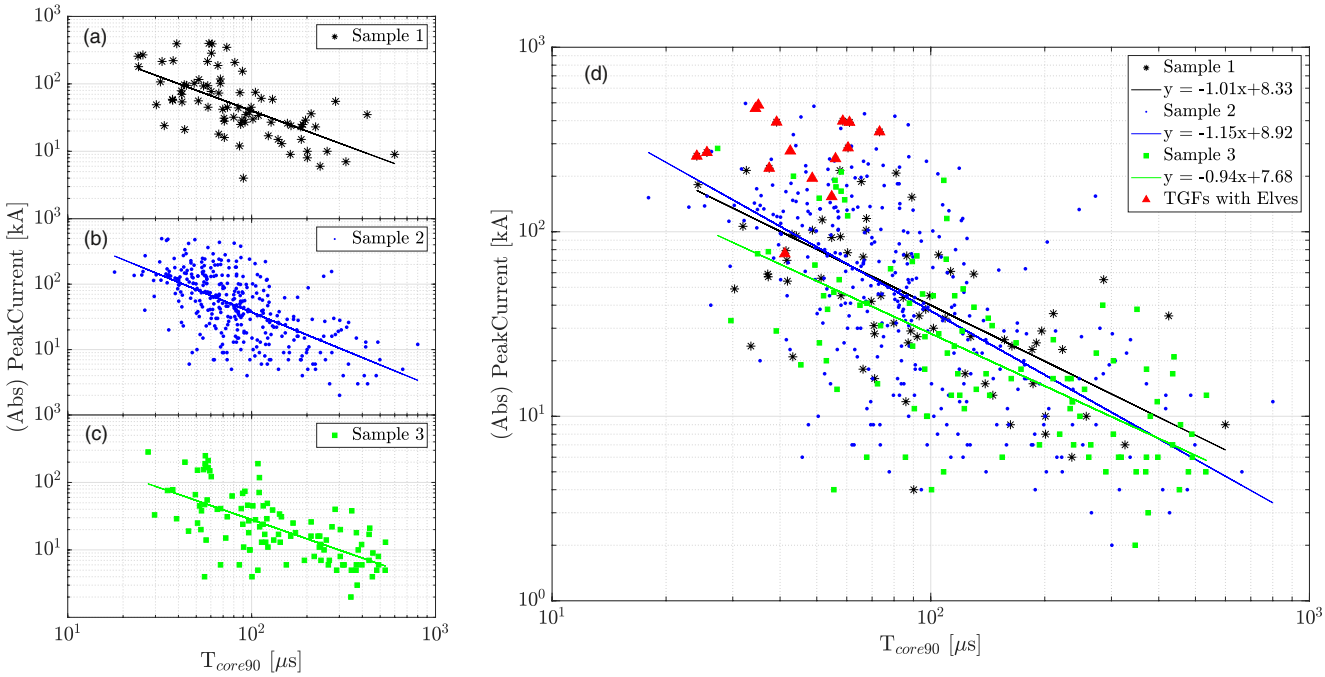

Figure 17. GLD360 peak current versus Terrestrial Gamma-ray Flash (TGF) core duration for the events in Samples 1, 2, and 3, shown in panels (a–c), with a linear regression line for each sample (log-log scale). In (d), all three samples are combined, and red triangles indicate the TGF-Elve pairs.

5.1. Selection of Events

Many of the 17 TGF-Elve pairs could easily be identified due to a strong UV pulse detection by MMIA, and a distinct pulse peak preceding the optical pulses in the 337 and 777.4 nm bands. Some events required more careful inspection of the pulse shapes to determine whether the UV pulse was more likely to originate from an Elve than from the lightning itself. For two of the 17 events (events 3 and 5), the photometer detections indicate that the TGF and Elve were produced outside the MMIA FOV, and that the Elve expanded into the FOV. The sferic locations were >100 km from the edge of the MMIA FOV, and the events were associated with particularly high peak currents (nearly 500 kA). Due to the much smaller FOV of MMIA compared to MXGS, a TGF with an Elve produced far outside the MMIA FOV will only be detected if the rings of the Elve are able to expand into the MMIA FOV. Hence, there could be events where the detected TGF is accompanied by an Elve although the UV signal is not detected by MMIA. In addition to these factors limiting the number of observations of TGF-Elve pairs by ASIM, it is also limited by MMIA only operating during nighttime, whereas MXGS operates during both day and night (Chanrion et al., 2019).

5.2. Uncertainties of Peak Current Estimates and Sferic Locations

Three (events 6, 15 and 17) of the 17 events were accompanied by two GLD360-detected sferics less than 300 μs apart. For two of them (event 6 and 17), the last of the two sferic detections was reported with a negative peak current with a larger absolute value than the first detection. Given the short time separation of the detections, these peak currents were likely from the ionospheric reflections of the current pulse associated with the event, and we refer to the first positive peak current value in Table 2. For the third event (event 15) with two sferics very close in time, the peak current of the second detection was also labeled with a positive polarity. However, the full waveform information from ENTLN indicates that this was just one stroke, and that it was reported twice by GLD360. In addition, the peak current value provided by ENTLN was closer to the first value (155 kA) than the second value (272 kA) reported by GLD360, and consequently we refer to 155 kA for this event in Table 2.

Table 3
Peak Currents for Different Duration Intervals

T_{core90}	Median peak current
[0, 56) μs	111 kA
[56, 140) μs	43 kA
[140, ∞) μs	13 kA

Table 4
Correlation Coefficient Between the Logarithmic Values of T_{core90} and Peak Current Presented in Figure 17

Sample	Number of events	Correlation coefficient	95% confidence interval
1	78	−0.64	[−0.75, −0.49]
2	349	−0.62	[−0.68, −0.55]
3	109	−0.66	[−0.75, −0.53]

5.3. Geographic Location of TGFs With Elves

With the exception of one event (event 2), the TGFs with Elves were associated with lightning occurring either over ocean or coastal regions, despite most lightning occurring over land (C. Liu et al., 2010; Peterson et al., 2017). Although our sample is small, our results agree with results presented by Chen et al. (2008), that Elves occur much more frequently over ocean and coastal regions than over land. Their study included over 5,400 Elves, and 91% of the Elves were detected over ocean or coastal regions. Results by Mach et al. (2010), Hutchins et al. (2013) and Said et al. (2013) also place the stronger negative CG lightning strokes over ocean regions. Stronger strokes being located over ocean regions are also highlighted in our Figure 15, where we show the distribution of peak currents associated with a large sample of ASIM TGFs (Samples 1, 2, and 3).

5.4. Peak Currents of TGFs/Elves

Through comparisons with a large set of GLD360 sferics, we found that the peak currents for the TGFs with Elves have positive polarity and fall into the high end of the peak current distribution for all lightning, in particular for the TGFs detected over ocean. The peak current values associated with the 15 events are all >75 kA, with a median value of ≈270 kA, whereas the median peak current (absolute) value for a large set of GLD360 sferics (shown in Figure 9) was 10 kA. This agrees with previous research showing that Elves tend to be associated with high peak currents (Chen et al., 2008; Inan et al., 1996; Marshall et al., 2015).

5.5. TGF Duration for the TGFs With Elves Compared to All TGFs

We show that in addition to the TGFs with Elves being associated with very high peak current values, they are also among the shortest TGFs detected by ASIM. Our results support modeling results by N. Liu et al. (2017), and equations outlined by Dwyer et al. (2012) and Dwyer and Cummer (2013), connecting short TGF durations and high peak currents. Short TGFs are related to more rapidly varying current moments, and can radiate stronger EMPs that are more likely to produce Elves (Rowland et al., 1995; N. Liu et al., 2017). TGFs with Elves appear to form a subset of events in one end of the distribution of peak currents associated with ASIM TGFs versus TGF core durations presented in Figure 17d. This suggests that, in general, we could expect a short TGF associated with a very high peak current to be accompanied by an Elve.

5.6. TGF Duration and Peak Currents

By comparing the peak currents associated with ASIM TGFs to the large set of GLD360 sferics from 2020, we found a similar tendency of there being fewer events with high peak currents than with low peak currents. However, for the large set of GLD360 sferics, there is a larger fraction of low peak current sferics than observed for the sferics associated with TGFs. The median (absolute value) peak current associated with ASIM TGFs is ∼40 kA (and a mean value of 75 kA), which is four times higher than the median peak current of the large GLD360 sferic set (using absolute values). However, the distribution also shows that TGFs are associated not only with high peak current lightning discharges; they can be associated with lightning discharges with a wide range of peak currents. This is consistent with the results by Mailyan et al. (2020), for TGFs detected by Fermi with simultaneous (within ±200 μs of the TGF onset) EMPs reported by GLD360.

As shown in Figure 17 and in Tables 3 and 4, all the three samples show that longer TGFs are associated with lower median peak current values. As outlined in Section 3.2, the samples represent different levels of reliability, but the linear fits, the correlation coefficients and their confidence intervals all give the same trend. The consistency check was especially important for indicating the most likely sferic candidate for the events in Sample 3, when there were several possible sferic detections within [−10, 40] ms and a radial distance of 800 km from the footpoint. Adding Sample 3 events that failed the consistency check to the sample resulted in a worse correlation coefficient between the absolute value peak currents and the core duration, and caused the trend to deviate more

from Sample 1, which had the highest reliability of the sferic association. Additionally, the 95% confidence interval was slightly wider. This further supports that the consistency check successfully excluded most of the unlikely sferic associations.

Using TGFs detected by Fermi and sferics detected by WWLLN, Connaughton et al. (2013) showed that short TGFs are more likely to have associated sferic detections than long TGFs. This relation was also confirmed by Lindanger et al. (2020) for TGFs detected by AGILE and associated WWLLN sferics, and by Mailyan et al. (2020) for Fermi TGFs and GLD360. Although we present our results differently and use a core duration instead of T_{50}, as was used by Connaughton et al. (2013), the trend is observed also for ASIM TGFs; a higher fraction of TGFs with shorter durations have associated sferic detections. Both panels of Figure 12 show a general decrease in the TGF-sferic matchrate with increasing core duration, with the trend being more evident in Figure 12a, where Sample 3 is excluded. The difference between the two panels is likely due to Sample 3 containing more false TGF-sferic matches. The general trend suggests that short TGFs are associated with fast current changes and could be related to the radiation of energy at frequencies that are more easily detected by the networks, with the amplitude of the radiation being proportional to the current moment derivative, which is much larger when shorter TGFs are observed (Dwyer & Cummer, 2013; Mezentsev et al., 2018).

Approximately 30% of the TGFs were not associated with any GLD360 sferics, which could be caused by several different factors. One explanation for an absent sferic match could be the network's detection efficiency at the location of the lightning discharge. Since the trend in Figure 17 is very visible for all three samples, it is more likely that the missing sferic match is due to small currents or slow rise-times of the current pulses (hence a small current derivative), reducing the chance of being picked up by the network. The median value of 39 kA is dependent on the threshold of the network, and would likely be lower (both for TGFs and for lightning) if the network was more sensitive.

In Figure 15a we present the locations of all TGFs (and the TGFs with Elves) relative to the shoreline, and show that the TGFs associated with the highest peak currents were more frequently found over ocean. In particular, the peak currents above ±300 kA were observed over ocean and coastal regions, including the TGFs with Elves. This is emphasized in Figures 15b and 15c, with TGFs associated with high peak currents occurring more frequently over ocean and coastal regions, indicating that this could be a property of both Elves and TGFs.

TGFs with sferic matches with very high peak currents could be associated with EIPs, especially the ones with accompanying Elves (Lyu et al., 2015). N. Liu et al. (2017) showed, through simulations, that EMPs radiated by EIPs can produce bright Elves. Event 4, occurring on the 8th of February 2019, was shown by Østgaard et al. (2021) to be accompanied by an EIP. Lyu et al. (2015) studied events with peak currents >200 kA, and found that the EIPs typically last 50–100 μs. With the exception of two events (event 10 and 15) presented in this paper, the TGFs with Elves were associated with peak current values above 200 kA. It is therefore very likely to have a TGF and an Elve when an EIP is observed. With regards to the full sample of TGFs with associated sferics (Samples 1, 2, and 3), only a very small amount was associated with the high peak currents of EIPs, implying that large number of TGFs are not associated with EIPs, as also indicated by Lyu et al. (2016). The distributions we present also show that TGFs can be associated with very high peak current values (>400 kA), in agreement with results by Cummer et al. (2014). Of the 536 TGFs within Samples 1, 2, and 3, only seven were associated with peak currents above 400 kA. Two of these TGFs were found to be accompanied by Elves, and for the remaining five there was no available MMIA data. Because of the very high peak currents of the associated sferics, these TGFs could also be accompanied by Elves.

6. Conclusion

Because of ASIM's unique ability to monitor both TGFs and TLEs, we were able to identify 17 TGFs accompanied by Elves. Using data from several ground-based lightning detection networks, but mainly from GLD360, we obtained information about the lightning discharges associated with the events and also with a large set of ASIM TGFs. From our observations we can conclude the following:

1. TGFs with accompanying Elves have short durations.

2. TGFs with Elves are associated with high peak current lightning. All events but one have peak currents >150 kA. The peak currents are higher than those associated with typical sferics and higher than those associated with other TGFs detected by ASIM.
3. 16 out of 17 TGFs are produced in coastal regions (±150 km of the shoreline) or over oceans.
4. For ∼30% of the TGFs there were no associated GLD360 sferics. These TGFs have longer durations (median: 150 μs) compared to those with associated sferics (median: 84 μs).
5. TGFs can be associated with a wide range of peak current values, but their sferic associations have a higher median peak current value than other sferic detections by GLD360. This could be influenced by the fact that we do not have the sensitivity to detect sferics associated with long TGFs.
6. There is a clear relation between TGF duration and peak current values; short duration TGFs tend to be associated with higher peak currents.

Data Availability Statement

ASIM data are available via the ASIM Science Data Center homepage (https://asdc.space.dtu.dk/). The data used to produce the figures in this paper are uploaded to Zenodo: https://doi.org/10.5281/zenodo.6457655 (Bjørge-Engeland, 2022).

Acknowledgments
This study was supported by the European Research Council under the European Union's Seventh Framework Programme (FP7/2007–2013)/ERC grant agreement no. 320839 and the Research Council of Norway under contracts 223252/F50 (CoE). The authors thank the International Space Science Institute, Bern, Switzerland, for providing financial support and meeting facilities in the frame of the International Team no. 471: Understanding the Properties of the Terrestrial Gamma-Ray Flash Population. The authors wish to thank VAISALA for the GLD360 lightning data, the WWLLN team, and the institutions contributing to WWLLN. The authors also wish to thank Earth Networks for providing lightning data. Atmosphere-Space Interactions Monitor is a mission of the European Space Agency and is funded by national grants of Denmark, Norway and Spain.

References

Albrechtsen, K. H., Østgaard, N., Berge, N., & Gjesteland, T. (2019). Observationally weak TGFs in the RHESSI data. *Journal of Geophysical Research: Atmospheres*, *124*, 287–298. https://doi.org/10.1029/2018JD029272

Bethe, H., & Heitler, W. (1934). On the stopping of fast particles and on the creation of positive electrons. *Proceedings of the Royal Society of London*, *146*(856), 83–112. https://doi.org/10.1098/rspa.1934.0140

Bjørge-Engeland, I. (2022). Supporting information for the paper: Terrestrial Gamma-ray flashes with accompanying elves detected by ASIM (Version 1) [dataset]. Zenodo. https://doi.org/10.5281/zenodo.6457655

Bui, V., Chang, L.-C., & Heckman, S. (2015). A performance study of Earth networks total lightning network (ENTLN) and worldwide lightning location network (WWLLN). *International Conference on Computational Science and Computational Intelligence*, 386–391. https://doi.org/10.1109/CSCI.2015.120

Bürgesser, R. E. (2017). Assessment of the World wide lightning location network (WWLLN) detection efficiency by comparison to the lightning imaging sensor (LIS). *Quarterly Journal of the Royal Meteorological Society*, *143*(708), 2809–2817. https://doi.org/10.1002/qj.3129

Carlson, B. E., Lehtinen, N. G., & Inan, U. S. (2007). Constraints on terrestrial gamma ray flash production from satellite observation. *Geophysical Research Letters*, *34*(8), 1–5. https://doi.org/10.1029/2006GL029229

Chanrion, O., Neubert, T., Lundgaard Rasmussen, I., Stoltze, C., Tcherniak, D., Jessen, N. C., et al. (2019). The modular multispectral imaging array (MMIA) of the ASIM payload on the international space station. *Space Science Reviews*, *215*(4), 28. https://doi.org/10.1007/s11214-019-0593-y

Chen, A. B., Kuo, C. L., Lee, Y. J., Su, H. T., Hsu, R. R., Chern, J. L., et al. (2008). Global distributions and occurrence rates of transient luminous events. *Journal of Geophysical Research*, *113*(8), 1–8. https://doi.org/10.1029/2008JA013101

Connaughton, V., Briggs, M. S., Xiong, S., Dwyer, J. R., Hutchins, M. L., Grove, J. E., et al. (2013). Radio signals from electron beams in terrestrial gamma ray flashes. *Journal of Geophysical Research: Space Physics*, *118*, 2313–2320. https://doi.org/10.1029/2012JA018288

Cummer, S. A., Lyu, F., Dwyer, J. R., Solanki, R., Briggs, M. S., Xiong, S., et al. (2014). The source altitude, electric current, and intrinsic brightness of terrestrial gamma ray flashes. *Geophysical Research Letters*, *41*(23), 8586–8593. https://doi.org/10.1002/2014GL062196

Cummer, S. A., Zhai, Y., Hu, W., Smith, D. M., Lopez, L. I., & Stanley, M. A. (2005). Measurements and implications of the relationship between lightning and terrestrial gamma ray flashes. *Geophysical Research Letters*, *32*(8), 1–5. https://doi.org/10.1029/2005GL022778

Cummins, K. L., Murphy, M., Demetriades, N., Pifer, B., Pessi, A., & Businger, S. (2008). *Modeling and calibration of Vaisala's operational long range lightning detection network*. Paper presented at 20th international lightning detection conference, and 2nd international lightning meteorology conference, Tucson AZ.

Dwyer, J. R., & Cummer, S. A. (2013). Radio emissions from terrestrial gamma-ray flashes. *Journal of Geophysical Research: Space Physics*, *118*, 3769–3790. https://doi.org/10.1002/jgra.50188

Dwyer, J. R., Smith, D. M., & Cummer, S. A. (2012). High-energy atmospheric physics: Terrestrial gamma-ray flashes and related phenomena. *Space Science Reviews*, *173*(1–4), 133–196. https://doi.org/10.1007/s11214-012-9894-0

Fishman, G. J., Meegan, C. A., Wilson, R. B., Brock, M. N., Horack, J. M., Kouveliotou, C., et al. (1994). The first BATSE gamma-ray burst catalog. *The Astrophysical Journal - Supplement Series*, *92*, 229. https://doi.org/10.1086/191968

Fukunishi, H., Takahashi, Y., Sakanoi, K., Inan, U. S., & Lyons, W. A. (1996). Elves: Lightning-induced transient luminous events in the lower ionosphere. *Geophysical Research Letters*, *23*(16), 2157–2160. https://doi.org/10.1029/96gl01979

Gjesteland, T., Østgaard, N., Collier, A. B., Carlson, B. E., Cohen, M. B., & Lehtinen, N. G. (2011). Confining the angular distribution of terrestrial gamma ray flash emission. *Journal of Geophysical Research*, *116*(11), 1–8. https://doi.org/10.1029/2011JA016716

Hazelton, B. J., Grefenstette, B. W., Smith, D. M., Dwyer, J. R., Shao, X. M., Cummer, S. A., et al. (2009). Spectral dependence of terrestrial gamma-ray flashes on source distance. *Geophysical Research Letters*, *36*(1), 1–5. https://doi.org/10.1029/2008GL035906

Heumesser, M., Chanrion, O., Neubert, T., Christian, H. J., Dimitriadou, K., Gordillo-Vazquez, F. J., et al. (2021). Spectral observations of optical emissions associated with terrestrial Gamma-Ray flashes. *Geophysical Research Letters*, *48*(4), 1–10. https://doi.org/10.1029/2020GL090700

Hutchins, M. L., Holzworth, R. H., Brundell, J. B., & Rodger, C. J. (2012). Relative detection efficiency of the World wide lightning location network. *Radio Science*, *47*(6), 1–9. https://doi.org/10.1029/2012RS005049

Hutchins, M. L., Holzworth, R. H., Virts, K. S., Wallace, J. M., & Heckman, S. (2013). Radiated VLF energy differences of land and oceanic lightning. *Geophysical Research Letters*, *40*(10), 2390–2394. https://doi.org/10.1002/grl.50406

Inan, U. S., Barrington-Leigh, C., Hansen, S., Glukhov, V. S., Bell, T. F., & Rairden, R. (1997). Rapid lateral expansion of optical luminosity in lightning-induced ionospheric flashes referred to as 'elves. *Geophysical Research Letters*, *24*(5), 583–586. https://doi.org/10.1029/97GL00404

Inan, U. S., Bell, T. F., & Rodriguez, J. V. (1991). Heating and ionization of the lower ionosphere by lightning. *Geophysical Research Letters*, *18*(4), 705–708. https://doi.org/10.1029/91gl00364

Inan, U. S., Sampson, W. A., & Taranenko, Y. N. (1996). Space-time structure of optical flashes and ionization changes produced by lighting-EMP. *Geophysical Research Letters*, *23*(2), 133–136. https://doi.org/10.1029/95GL03816

Köhn, C., & Ebert, U. (2014). Angular distribution of Bremsstrahlung photons and of positrons for calculations of terrestrial gamma-ray flashes and positron beams. *Atmospheric Research*, *135–136*, 432–465. https://doi.org/10.1016/j.atmosres.2013.03.012

Lindanger, A., Marisaldi, M., Maiorana, C., Sarria, D., Albrechtsen, K., Østgaard, N., et al. (2020). The 3rd AGILE terrestrial Gamma Ray flash catalog. Part I: Association to lightning sferics. *Journal of Geophysical Research: Atmospheres*, *125*, e2019JD031985. https://doi.org/10.1029/2019jd031985

Lindanger, A., Marisaldi, M., Sarria, D., Østgaard, N., Lehtinen, N., Skeie, C. A., et al. (2021). Spectral analysis of individual terrestrial Gamma-ray flashes detected by ASIM. *Journal of Geophysical Research: Atmospheres*, *126*, 1–18. https://doi.org/10.1029/2021jd035347

Liu, C., Williams, E. R., Zipser, E. J., & Burns, G. (2010). Diurnal variations of global thunderstorms and electrified shower clouds and their contribution to the global electrical circuit. *Journal of the Atmospheric Sciences*, *67*(2), 309–323. https://doi.org/10.1175/2009JAS3248.1

Liu, N., Dwyer, J. R., & Cummer, S. A. (2017). Elves accompanying terrestrial Gamma Ray flashes. *Journal of Geophysical Research: Space Physics*, *122*, 563–610. https://doi.org/10.1002/2017JA024344

Lu, G., Blakeslee, R. J., Li, J., Smith, D. M., Shao, X. M., McCaul, E. W., et al. (2010). Lightning mapping observation of a terrestrial gamma-ray flash. *Geophysical Research Letters*, *37*(11), 1–5. https://doi.org/10.1029/2010GL043494

Lyu, F., Cummer, S. A., Briggs, M., Marisaldi, M., Blakeslee, R. J., Bruning, E., et al. (2016). Ground detection of terrestrial gamma ray flashes from distant radio signals. *Geophysical Research Letters*, *43*(16), 8728–8734. https://doi.org/10.1002/2016GL070154

Lyu, F., Cummer, S. A., & McTague, L. (2015). Insights into high peak current in-cloud lightning events during thunderstorms. *Geophysical Research Letters*, *42*(16), 6836–6843. https://doi.org/10.1002/2015GL065047

Mach, D. M., Blakeslee, R. J., & Bateman, M. G. (2011). Global electric circuit implications of combined aircraft storm electric current measurements and satellite-based diurnal lightning statistics. *Journal of Geophysical Research*, *116*, 1–13. https://doi.org/10.1029/2010JD014462

Mach, D. M., Blakeslee, R. J., Bateman, M. G., & Bailey, J. C. (2010). Comparisons of total currents based on storm location, polarity, and flash rates derived from high-altitude aircraft overflights. *Journal of Geophysical Research*, *115*, 1–19. https://doi.org/10.1029/2009JD012240

Mailyan, B. G., Nag, A., Dwyer, J. R., Said, R. K., Briggs, M. S., Roberts, O. J., et al. (2020). Gamma-Ray and Radio-frequency Radiation from thunderstorms observed from space and Ground. *Scientific Reports*, *10*(1), 1–9. https://doi.org/10.1038/s41598-020-63437-2

Maiorana, C., Marisaldi, M., Lindanger, A., Østgaard, N., Ursi, A., Sarria, D., et al. (2020). The 3rd AGILE Terrestrial Gamma-ray Flashes Catalog. Part II: Optimized selection criteria and characteristics of the new sample. *Journal of Geophysical Research: Atmospheres*, *125*, e2019JD031986. https://doi.org/10.1029/2019jd031986

Marshall, R. A., Da Silva, C. L., & Pasko, V. P. (2015). Elve doublets and compact intracloud discharges. *Geophysical Research Letters*, *42*(14), 6112–6119. https://doi.org/10.1002/2015GL064862

Mezentsev, A., Lehtinen, N., Østgaard, N., Pérez-Invernón, F. J., & Cummer, S. A. (2018). Spectral characteristics of VLF sferics associated with RHESSI TGFs. *Journal of Geophysical Research: Atmospheres*, *123*, 139–159. https://doi.org/10.1002/2017JD027624

Neubert, T., Østgaard, N., Reglero, V., Blanc, E., Chanrion, O., Oxborrow, C. A., et al. (2019). The ASIM mission on the international space station. *Space Science Reviews*, *215*(2), 26. https://doi.org/10.1007/s11214-019-0592-z

Neubert, T., Østgaard, N., Reglero, V., Chanrion, O., Heumesser, M., Dimitriadou, K., et al. (2020). Ultraviolet emissions powered by lightning. *Science*, *186*, 183–186. https://doi.org/10.1126/science.aax3872

Østgaard, N., Balling, J. E., Bjørnsen, T., Brauer, P., Budtz-Jørgensen, C., Bujwan, W., et al. (2019). The modular X- and Gamma-Ray sensor (MXGS) of the ASIM payload on the international space station. *Space Science Reviews*, *215*(2), 23. https://doi.org/10.1007/s11214-018-0573-7

Østgaard, N., Cummer, S. A., Mezentsev, A., Luque, A., Dwyer, J., Neubert, T., et al. (2021). Simultaneous observations of EIP, TGF, Elve, and optical lightning. *Journal of Geophysical Research: Atmospheres*, *126*, e2020JD033921. https://doi.org/10.1029/2020JD033921

Østgaard, N., Gjesteland, T., Carlson, B. E., Collier, A. B., Cummer, S. A., Lu, G., & Christian, H. J. (2013). Simultaneous observations of optical lightning and terrestrial gamma ray flash from space. *Geophysical Research Letters*, *40*(10), 2423–2426. https://doi.org/10.1002/grl.50466

Østgaard, N., Gjesteland, T., Stadsnes, J., Connell, P. H., & Carlson, B. (2008). Production altitude and time delays of the terrestrial gamma flashes: Revisiting the Burst and Transient Source Experiment spectra. *Journal of Geophysical Research*, *113*(2), 1–14. https://doi.org/10.1029/2007JA012618

Østgaard, N., Neubert, T., Reglero, V., Ullaland, K., Yang, S., Genov, G., et al. (2019b). First 10 Months of TGF observations by ASIM. *Journal of Geophysical Research: Atmospheres*, *124*, 14024–14036. https://doi.org/10.1029/2019JD031214

Pasko, V. P., Yair, Y., & Kuo, C. L. (2012). Lightning related transient luminous events at high altitude in the Earth's atmosphere: Phenomenology, mechanisms and effects. *Space Science Reviews*, *168*(1–4), 475–516. https://doi.org/10.1007/s11214-011-9813-9

Peterson, M., Deierling, W., Liu, C., Mach, D., & Kalb, C. (2017). The properties of optical lightning flashes and the clouds they illuminate. *Journal of Geophysical Research: Atmospheres*, *122*, 423–442. https://doi.org/10.1002/2016JD025312

Rowland, H. L., Fernsler, R. F., Huba, J. D., & Bernhardt, P. A. (1995). Lightning driven EMP in the upper atmosphere. *Geophysical Research Letters*, *22*(4), 361–364. https://doi.org/10.1029/95GL00012

Rudlosky, S. D., Peterson, M. J., & Kahn, D. T. (2017). GLD360 performance relative to TRMM LIS. *Journal of Atmospheric and Oceanic Technology*, *34*(6), 1307–1322. https://doi.org/10.1175/JTECH-D-16-0243.1

Rudlosky, S. D., & Shea, D. T. (2013). Evaluating WWLLN performance relative to TRMM/LIS. *Geophysical Research Letters*, *40*(10), 2344–2348. https://doi.org/10.1002/grl.50428

Said, R. K., Cohen, M. B., & Inan, U. S. (2013). Highly intense lightning over the oceans: Estimated peak currents from global GLD360 observations. *Journal of Geophysical Research: Atmospheres*, *118*, 6905–6915. https://doi.org/10.1002/jgrd.50508

Said, R. K., Inan, U. S., & Cummins, K. L. (2010). Long-range lightning geolocation using a VLF radio atmospheric waveform bank. *Journal of Geophysical Research*, *115*, 1–19. https://doi.org/10.1029/2010JD013863

Said, R., & Murphy, M. (2016, April). *GLD360 upgrade: Performance analysis and applications*. Paper presented at 24th international lightning detection conference, San Diego, CA.

Shao, X. M., Hamlin, T., & Smith, D. M. (2010). A closer examination of terrestrial gamma-ray flash-related lightning processes. *Journal of Geophysical Research*, *115*(6), 1–8. https://doi.org/10.1029/2009JA014835

Stanley, M. A., Shao, X. M., Smith, D. M., Lopez, L. I., Pongratz, M. B., Harlin, J. D., et al. (2006). A link between terrestrial gamma-ray flashes and intracloud lightning discharges. *Geophysical Research Letters*, *33*(6), 1–5. https://doi.org/10.1029/2005GL025537

Zhu, Y., Rakov, V. A., Tran, M. D., Stock, M. G., Heckman, S., Liu, C., et al. (2017). Evaluation of ENTLN performance characteristics based on the ground truth natural and rocket-triggered lightning data acquired in Florida. *Journal of Geophysical Research: Atmospheres*, *122*, 9858–9866. https://doi.org/10.1002/2017JD027270